NJC

Accepted Manuscript

This is an *Accepted Manuscript*, which has been through the Royal Society of Chemistry peer review process and has been accepted for publication.

Accepted Manuscripts are published online shortly after acceptance, before technical editing, formatting and proof reading. Using this free service, authors can make their results available to the community, in citable form, before we publish the edited article. We will replace this *Accepted Manuscript* with the edited and formatted *Advance Article* as soon as it is available.

You can find more information about *Accepted Manuscripts* in the Information for Authors.

Please note that technical editing may introduce minor changes to the text and/or graphics, which may alter content. The journal's standard Terms & Conditions and the Ethical guidelines still apply. In no event shall the Royal Society of Chemistry be held responsible for any errors or omissions in this *Accepted Manuscript* or any consequences arising from the use of any information it contains.

ROYAL SOCIETY OF CHEMISTRY

www.rsc.org/njc

The electrochemical synthesis of Pt particles on ZrO_2-ERGO modified electrodes with high electrocatalytic performance for methanol oxidation

A.T. Ezhil Vilian[a], Shen-Ming Chen[a]*, Shakkthivel Piraman [b],

[a]Department of Chemical Engineering and Biotechnology, National Taipei University of Technology, No.1, Section 3, Chung-Hsiao East Road, Taipei 106, Taiwan (R.O.C).

[b]Sustainable and Smart Materials Research Lab., Department of Nano Science and Technology, Alagappa University, Karaikudi 630 002, Tamil Nadu, India

*Corresponding author. Fax: +886 2270 25238; Tel: +886 2270 17147, E-mail: smchen78@ms15.hinet.net

Abstract

We report on a process for the electrochemical synthesis of Pt particles on a composite of zirconium oxide/electrochemically reduced graphene oxide (ERGO) sheet. The zirconium oxide produces bridging molecules which allow easy anchoring of Pt particles to form a functional ERGO multilayer film produced through a co-electrochemical deposition procedure. The catalytic performance improves as a consequence of the addition of ZrO_2, which increases the number of active Pt sites. Scanning electron microscopy (SEM), Raman spectrometry, X-ray diffraction (XRD), and electrochemical impedance spectroscopy (EIS) are used to characterize the microstructure and morphology of the synthesized Pt/ZrO_2-ERGO electrode. It is found that this approach allows for the development of new kinds of electro catalysts for use in direct methanol fuel cells. The process of methanol oxidation is investigated through cyclic voltammetry and amperometry. The results indicate that the Pt/ZrO_2-ERGO electro catalyst exhibits much higher catalytic activity and better stability than either the Pt/ERGO or commercially available Pt/C electro catalysts as well as better tolerance to CO during the electro-oxidation of methanol. The Pt catalysts on the ZrO_2-ERGO composite facilitate the methanol oxidation reaction making this a promising material for application in the direct methanol fuel cells that are used in the fields of biotechnology and environmental chemistry.

Keywords: Electrochemically reduced graphene oxide, Pt particle, Electrocatalytic activity, Methanol oxidation, Zirconium oxide.

1. Introduction

Direct methanol fuel cells (DMFCs) are attracting increasing attention in both academia and industry as green power sources for vehicles and portable electronics, because they can convert chemical energy directly into electrical energy.[1-3] However, the commercial application of DMFCs is still hindered by the sky-rocketing prices of scarce materials needed for their fabrication such as the Pt catalyst and the sluggish methanol oxidation reaction.[4,5] Therefore, substitutes for the carbon-based Pt catalysts are urgently needed, and improved Pt utilization and catalytic activity are the main issues for methanol fuel cell researchers.[6] A variety of strategies have been used to solve these problems, including optimizing the size and shape of the Pt nanoparticles, developing Pt nanoparticles with high energy facets and alloying Pt with its neighboring transition metals such as Ru, Ni, Pd and Au. Pt nanoparticles have been used on different types of catalyst supports including carbon black, carbon nanotubes and mesoporous carbon.[7,8] Although different methods for the preparation of Pt based composites and the exhibited catalytic performance have been discussed in previous studies, a facile method for the production of Pt NPs with well-controlled dimensions and morphologies and effective loading remains a challenging task.[9]

Recently, the unique properties of graphene, which is a new kind of carbon material with a single layer of bonded-sp^2 carbons compacted into a two-dimensional honeycomb lattice, have attracted intense interest. Its extremely high surface area, excellent electrical conductivity and superior chemical stability make graphene a favorable candidate for electro catalyst supports in DMFCs.[10-12] Graphene oxide (GO) has many oxygen-containing functional groups, such as

hydroxyl, epoxide, carbonyl, and carboxyl groups, on its surface. These features give GO good solubility in aqueous solvents, even some organic solvents, allowing the creation of more active sites for supporting metal oxides (e.g., MnO_2, TiO_2, WO_3, CeO_2, Fe_2O_3) which could have synergic effects to improve the performance of the catalysts.[13-16]

Zirconium oxide (ZrO_2) nanomaterials are also industrially important because of their unique combination of properties like thermal stability, chemical inertness, and lack of toxicity.[17-19] In the present study, ZrO_2 nanostructures are an excellent candidate material for use in various applications, such as fuel cells, optical coatings, flat panel displays with low-energy excitation sources, solar energy converters, optical amplifiers, photonic devices, and so on.[20-23]

To the best of our knowledge, there have been no studies on the use of platinum particle decorated ZrO_2-ERGO composites as supports for high electron and proton conductivity. To fill this gap, this study investigates the electrochemical behavior and electrocatalytic activity of an Pt/ZrO_2-ERGO electrode for methanol oxidation. It is found that the electrochemically active surface areas of Pt/ZrO_2-ERGO is higher than for the Pt/ERGO or the commercially available Pt/C electro catalysts. The Pt/ZrO_2-ERGO modified electrode has a higher electrocatalytic activity, leading to better performance and should be suitable for application in highly stable methanol fuel cells. In this study, a Pt/ZrO_2-ERGO modified electrode is used as the anode and Nafion 112 as the membrane. During subsequent testing of the direct methanol fuel cell it was found to have a maximum power density of 125mW cm^{-2} at 30 °C.

2. Experimental procedure

2.1 Chemicals

Graphite powder (<20 μm), zirconyl chloride octahydrate ($ZrOCl_2$), potassium hexachloroplatinate (IV), Nafion 112, and commercial Pt/C were purchased from Sigma-Aldrich while the perchloric acid ($HClO_4$) and methanol was purchased from Wako Chemicals. All other chemicals were of analytical grade. Deionized water was obtained from a Millipore Milli-Q purification system (18.2 M Ω cm).

2.2 Apparatus

The electrochemical activity of the electro catalysts was evaluated by cyclic voltammetry (CV) using a three-electrode system and a CHI 405A model electrochemical workstation. The Pt/ZrO_2-ERGO working electrode was an electro catalyst modified GCE (geometric area = 0.07 cm^2). A saturated Ag/AgCl (sat. KCl) was used as the reference electrode and a platinum wire electrode served as the counter electrode. Electrochemical impedance spectroscopic measurements of the samples were performed (using an EIM6ex ZAHNER, Kroanch, Germany) in the frequency range of 0.1 Hz to 100 kHz. Scanning electron microscopy (SEM) was performed on the prepared composite with a Hitachi S-3000 H Scanning Electron Microscope. Energy-dispersive X-ray spectroscopy (EDX) was recorded for the composite films using a HORIBA EMAX X-ACT Model 51-ADD0009. The atomic force microscopic (AFM) images were collected with a multimode scanning probe microscope (Being Nano-Instruments CSPM-4000, China), the transmission electron microscopic (TEM) images were recorded using a Philips TECNAI 20 microscope (200 kV) and the Fourier transform infrared (FTIR) spectra were obtained using a Perkin Elmer RXI spectrometer. The Raman spectra were recorded using a Raman spectrometer (RENISHAW in Via system, U.K) using a 514.4 nm He/Ne laser. The as-prepared composite films were coated onto the ITO and then dried overnight prior to X-ray diffraction (XRD) analysis. The crystal structures of the product were characterized by the X-ray

diffraction system (PANalytical B.V., The Netherlands) using Cu Kα as the radiation source at an operating voltage of 40 kV and a scan rate of 60 min^{-1}. The current and power were measured using precision multimeters (Keithley instruments; model 2400) in a room temperature atmosphere.

2.3 Preparation of electro catalysts

The GO was synthesized from natural graphite powder (99.9%) by the well-known modified Hummer's method. [24] Briefly, 1 g of graphite was suspended in 2.5 g of $K_2S_2O_8$, after which 46 ml of H_2SO_4 were added followed by stirring in an ice-bath. Next, 2.5 g of P_2O_5 were added gradually during stirring and cooling, maintaining the temperature of the mixture was below 20 °C. Then 6 g of $KMnO_4$ and 1 g of $NaNO_3$ were slowly added to the beaker while the temperature was maintained below 20 ºC. The reaction was terminated by adding 250 ml of deionized water followed by 6 ml of H_2O_2 (30 weight %). The solid suspension was filtered, washed with a 2 M HCl solution and then 3-4 times more in ethanol and dried in a vacuum at 60 ºC overnight. Then, the graphene oxide (1g) was exfoliated in deionized water (1mL) during ultrasonic treatment for 1 hour to form a light-brown solution. Before modification, the bare glassy carbon electrode (GCE) with a diameter of 3 mm was polished with an alumina (particle size of about 0.05 mm)/water slurry using a Buehler polishing kit and washed ultrasonically in double distilled water before being dried. Then 5 µL of the as prepared GO suspension were dropped onto the surface of the pretreated GCE electrode and dried. Then GO modified electrode was transferred into a 0.05 M phosphate buffer solution comprised of 5.0 mM $ZrOCl_2$ in a PBS (pH 5). After this, 10 consecutive cyclic voltammograms were recorded with a potential ranging from 0 and -1.5 V at a scan rate of 20 mV s^{-1} (See S1.B). After this, the ZrO_2-ERGO/GCE was moved to an electrochemical cell containing 1 mM of K_2PtCl_6 in a 0.5 M H_2SO_4 solution then

recorded for 10 cycles with a potential range from -0.25 to 1.0 V (See S1.C). The Pt/ZrO_2-ERGO modified electrode was rinsed with double distilled water and dried using N_2. The CV measurements were carried out with a potential ranging from -0.2 to 1.0 V at a scan rate of 50 mV s^{-1} in both the 1M $HClO_4$ electrolyte solution and 1M $HClO_4$ + 1M CH_3OH electrolyte solution. A simple methanol fuel cell was constructed using the Pt/ZrO_2-ERGO modified GCE as an anode and the commercially available Pt/C as a cathode. Nafion 112 was used as the membrane in our homemade fuel cell setup in our laboratory. Using a concentration of 1 M methanol solution, the direct methanol fuel cell is reported to exhibit higher open circuit voltages and power density output. The synthesis and fabrication of Pt/ZrO_2-ERGO electro catalysts are illustrated in Scheme 1. Polarization and power curves were recorded in a 1 M methanol aqueous solution.

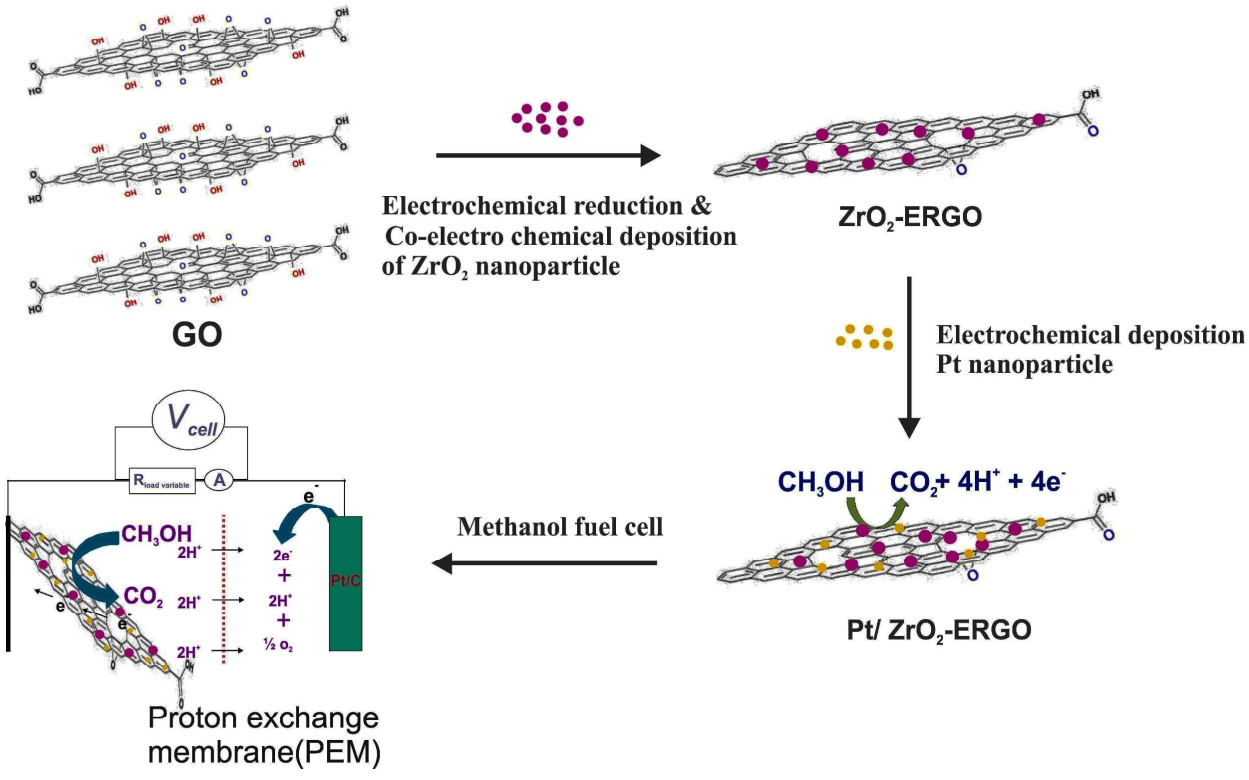

Scheme 1.Schematic representation of methanol oxidation taking place at the Pt/ZrO_2-ERGO electro catalyst modified electrode.

3. Results and discussion

3.1 Surface and composite analysis

Fig.1 shows some typical SEM images obtained for the ERGO/ITO, Pt/ERGO/ITO, and Pt/ZrO_2-ERGO/ITO electrodes. Fig. 1A displays an SEM image of the ERGO and corresponding EDX elemental analysis. One can see the typical ERGO flakes with broad lamellar structures or folds, which provide the larger surface-area. In addition, the EDX elemental analysis of the ERGO shows the presence of C (85%) and O (15%) as can be seen in Fig. 1D. The results clearly indicate that the electrochemical reduction has been effective. The oxygen functionalities and negative charges at the ERGO surface favor the adsorption of ZrO_2. Further removal of these oxygen-containing groups leads to a remarkable increase in ZrO_2 particle size due to aggregation. The oxygen-containing groups on the ERGO surface play an important role in enhancing the loading of ZrO_2. The SEM image in Fig. 1C displays small granular shaped ZrO_2 particles that have been deposited on the ERGO surface which provide a large surface area for the incorporation of the spherically shaped Pt particles. The Pt particles were well distributed on the surface of the ZrO_2-ERGO to form the Pt/ZrO_2-ERGO/ITO composite film. Furthermore, the composition of this Pt/ZrO_2-ERGO/ITO composite film was also confirmed by EDX spectroscopy (Fig. 1(F)) to be comprised of C (12%), O (66%), Zr (22%), and Pt (22%). All of the results suggest that the ZrO_2-ERGO was well covered by Pt particles. The morphology of the as prepared composite was further confirmed using HRTEM. Fig 1G shows an HRTEM image of the Pt/ZrO_2-ERGO electro catalyst. The Pt nanoparticles are spherical in shape while the ZrO_2

particles have grown into larger grains. The granular surface microstructures on the particles gave also disappeared reducing the porosity of the surface. The uniform distribution on the ERGO sheet is also shown. There is some corrugation and scrolling at the edges of the ERGO, but it can be clearly seen that the ERGO sheet is decorated with uniformly distributed spherical Pt/ZrO_2 nanoparticles. Fig. 1G shows the Pt/ZrO_2 nanoparticles anchored on the surface of both sides of the ERGO sheets. The good dispersion behavior and larger surface area, which provided more active sites and electrocatalytic reaction centers, make this a potential material for use in an electrochemical sensor.

Fig. 1

3.2 Characteristics of the Pt/ZrO_2-ERGOcomposite

Fig. 2A presents the FT-IR spectra of (a) GO and (b) Pt/ZrO_2-ERGO. The GO spectrum is in good agreement with that observed in previous work. [25] GO is a two-dimensional carbon sheet in which there exists a large amount of oxygen functional groups such as hydroxyl, carboxyl and epoxide groups. The broad peak for GO in Fig. 2 (a) at 3444.5 cm^{-1} can be ascribed to the stretching of O-H. [26] After reduction, as can be seen in the ERGO (Fig. S3(a)),the most intense peak at 1165 cm^{-1} displays the presence of C-O stretching vibration, and the second most intense peak at 1545 cm^{-1} corresponds to the C=C stretching for the skeletal in-plane vibration.The peaks in the range 2920 cm-1 to 2850 cm^{-1} corresponds to the asymmetric C-H stretching; in addition,a small peak positioned at 1736 cm^{-1} can be attributed to stretching vibration for C=O. Fig. S3 represent the FT-IR spectra of (b) ZrO_2-ERGO nanocomposite, the intensity of the peak at 1557 cm^{-1} gets maximized, which is due to the skeletal in-plane vibration of C=C, whereas it is less pronounced in RGO data, The reduction of GO was evidenced by the intensity decrease or even suppression of different oxygen functionalities. Which is a clear leads

to further reduction of the GO to RGO. On the other hands, there is a significant decrease in the intensity of these peaks in the FT-IR spectra for the Pt/ZrO_2-ERGO film, with some of them vanishing completely. This indicates that the bulk of the oxygen-containing functional groups were removed from the GO. A new peak can be observed at about 1560 cm^{-1} in the Pt/ZrO_2-ERGO spectra, which can be attributed to the skeletal vibration of the graphene sheets.

Fig. 2

The Raman spectra for GO, ZrO_2-ERGO and Pt/ZrO_2-ERGO are shown in Fig. 2B. For all three samples we observe two bands, which corresponds (the D band and the G band) in the Raman spectrum of GO, ZrO2-ERGO and Pt/ZrO_2-ERGO located at 1352 and 1585 cm^{-1}.The intensity ratio of the D band to the G band (ID/IG) for Pt/ZrO_2-ERGO correlates with the average size of the sp^2 domains, that is, the smaller the size of the sp^2 domains, the higher the ID/IG intensity ratio. From Fig. 2B, the intensity ratios of D and G bands (ID/IG) of GO (1.09) sample are obviously larger than that of ZrO_2-ERGO (1.16) which confirms that most of the oxygenated groups would have been removed during the electrochemical reduction process or which is regarded as the successful modification of ZrO_2 onto the ERGO sheets. On the other hands, the ID/IG ratio varies from 1.09 for GO to 1.38 for the Pt/ZrO_2-ERGO composites. [28] The intensity ratio of the D to G band (ID/IG) is generally accepted to reflect the defect density of carbonaceous material, which is more concentrated in Pt/ZrO_2-ERGO than in the GO. It can be concluded that the Pt/ZrO_2-ERGO showed the few-layer feature of graphene. Thus, the Raman results are consistent with the HRTEM characterization, clearly showing the few-layer feature of graphene.

Fig. 2C shows the XRD patterns for the Pt/ZrO_2-ERGO. A broad and weak (002) diffraction peak arising from the slight stacking of the graphene sheets is also detected at a 2θ of about 25°, confirming the successful reduction of GO into ERGO. The XRD patterns for the ZrO_2 particles in Fig. 2 C show diffraction peaks at 2θ = 30° (110), 38° (111) and 52° (220) which are characteristic of ZrO_2 particle structure, and indicative of the formation of ZrO_2 particles on the ERGO. [29] The peaks between 30° and 90° can be indexed to Pt crystals with a face-centered cubic (fcc) structure. The peaks at 2θ = 39.7°, 46.3°, and 67.6° are assigned to the (111), (200), and (220) planes of the Pt particles (according to the standard card for cubic Pt, JCPDS No. 04-0802). This indicates that alloying has occurred, caused by the incorporation of the smaller ZrO_2 particles into the Pt fcc structure .[30, 31] The average size of the Pt particles electrodeposited on the ZrO_2-ERGO was calculated using Scherrer's equation 1:

$$\mathbf{D}=\frac{0.9\lambda}{\beta\cos\theta_B}, \quad (1)$$

where d is the diameter (Å); λ is the wavelength of the X-ray (1.54056 Å); β is the full-width half-maximum of respective diffraction peaks; and θ_B is the angle at the peak maximum. The calculated average particle size of Pt particles on the ZrO_2-ERGO is about 20nm. This result is in good agreement with the AFM results. However, the AFM results reveal the Pt particles to have a spherical morphology (Fig. S**2** C). From the histogram of the size distribution, the average size of the Pt particles was found to center around 20 nm (Fig. S**2** D). The XRD results also indicate that Pt particles were obtained on the ZrO_2-ERGO sheets. The EDX measurements verify the existence of Pt on the ZrO_2-ERGO surface.

3.3 Electrochemical performance of the fabricated modified electrodes

Fig. 3A shows representative cyclic voltammetry (CV) curves for (a) Pt/C, (b) Pt/ZrO_2, (c) Pt/ERGO, and (d) Pt/ZrO_2-ERGO electro catalysts in a 1M $HClO_4$ solution. The scan rate was 50 mV s^{-1} between -0.2 V and 1.0 V, as shown in Fig. 3A. For comparison, the cyclic voltammograms of the Pt/C (34.02 m^2 /g), Pt/ZrO_2 (36.13 m^2 /g), Pt/ERGO (42.93 m^2 /g) and Pt/ZrO_2-ERGO (68.2 m^2 /g) electro catalysts are also presented. For the Pt/C, Pt/ZrO_2 electro catalyst, a poorly resolved peak is observed in the hydrogen adsorption/desorption region. The electrochemically active surface area (EAS) (m^2 g^{-1} Pt) of the Pt deposited on the surface of different modified electrodes is calculated according to the charge in hydrogen desorption (Q_H, mC cm^{-2}) as follows: [32]

$$\mathbf{EAS = Q_H/0.21}W_{Pt}, \quad \mathbf{(2)}$$

where W_{Pt} is the Pt loading (g cm^{-2}) on the surface of the different modified electrodes; and 0.21 is the charge (mC cm^{-2}) required to oxidize a monolayer of adsorbed hydrogen atoms on the platinum surface. The Pt/ZrO_2-ERGO electro catalyst exhibits a relatively broader peak with a slightly higher current in the adsorption/desorption region than the Pt/ERGO electro catalyst. It can be seen that Pt particles may originate from the more uniformly covered surface of the ZrO_2-ERGO composites. The smaller particles would be responsible for their good electrochemical catalytic performance. The results of the investigation of the activity of the Pt/ZrO_2-ERGO electro catalyst described in our work show well-defined hydrogen adsorption/desorption peaks with a much larger area in the potential region -0.2 V to 1.0 V, demonstrating the higher surface area of the electro catalyst. The greater surface area may be owed to the high deposition rate and small size of the Pt particles on the ZrO_2-ERGO composites. Furthermore, ZrO_2 increased the

concentration of the OH_{ads} species on the electro catalyst surface, and these OH_{ads} species then reacted with CO-like intermediate species to produce CO_2 products, releasing the active sites on the Pt for further electrochemical reaction. The mechanism for the methanol oxidation of the Pt/ZrO_2-ERGO electro catalysts should form Pt adsorbed carbonaceous intermediates (mainly CO) which are formulated as follows: [33]

$$OH^- + ZrO_2 \rightarrow ZrO_2 \text{ .}OH_{ads} + e^- \quad (3)$$

$$Pt\text{-}(CH_3OH_{ads}) + 4OH^- \rightarrow Pt\text{-}CO_{ads} + 4H_2O + 4e^- \quad (4)$$

Fig. (3)

Fig. 3B shows typical cyclic voltammograms of methanol oxidation for catalysis in a 1M $HClO_4$ solution, at a scan rate of 50 mV s^{-1} between -0.2 V and 1.0 V by the: (a) Pt/C, (b) Pt/ZrO_2, (c) Pt/ERGO, and (d) Pt/ZrO_2-ERGO electrodes. The peak current of the maximum current density of the forward peak (I_f) is related to the oxidation of freshly chemisorbed species issued from methanol adsorption, and that of the backward peak (I_b) represents the removal of carbonaceous species incompletely oxidized in the forward scan. The ratio of the maximum current to the peak anodic current (I_f/I_b) in the forward sweep to the reverse sweep is utilized in order to assess the electro catalyst's tolerance of the accumulation of intermediate species. The I_f/I_b ratio can be used to describe the CO tolerance of an electro catalyst for comparison to the accumulation of carbonaceous species such as CO on the electrode surface. A lower ratio of forward anodic peak current density (I_f) to the reverse anodic peak current density (I_b) indicates poor oxidation of methanol as opposed to CO_2 during the forward anodic scan with excessive accumulation of carbonaceous residues on the electro catalyst surface. Remarkably, a higher I_f/I_b value suggests that the electro catalysts are more efficient at lowering the adsorbed carbon

monoxide. The value is a useful way of comparing the long-term catalytic activity between different electro catalysts. As shown in Fig. 3B, the I_f/I_b ratio of the (d) Pt/ZrO_2-ERGO electro catalyst I_f/I_b value is 1.92; (c) the Pt/ERGO I_f/I_b value is 1.12; and (b) the Pt/ZrO_2 I_f/I_b value is 1.02, which is substantially higher than that of (a) the Pt/C I_f/I_b value is 0.98 (See Table 1). The results show the better catalytic tolerance of thes composites, and indicate lower accumulation of CO-like species on the electro catalyst during the methanol oxidation reaction, thus leading to excellent catalytic activity. A summary of the different modified electrodes and their I_f/I_b values is given in Table 2. The higher electrochemical performance observed here can probably be attributed to the higher utilization of Pt on the ZrO_2-ERGO. The greater surface area provided leads to higher electrocatalytic activity, most likely due to the large number of nucleation centers available on the surface of the ERGO. The unique structure of the support appears to cause the Pt on the ZrO_2-ERGO to have higher specific activity leading to the higher methanol oxidation performance. This represents a class of functional electro catalysts with promising properties for DMFCs.

Further investigation was done to explore the transport characteristics and electrocatalytic oxidation of methanol on the Pt/ZrO_2-ERGO electrodes in the 1M $HClO_4$ + 1M CH_3OH aqueous solutions at different sweep rates. Fig. 3C shows the dependence curve of the peak currents for the square root of the scan rates. The peak currents are linearly proportional to the square root of the scan rates. In addition, the Ep moves to slightly higher potentials with an increasing scan rate, which suggests that the electrocatalytic oxidation of methanol on Pt/ZrO_2-ERGO electrodes is a diffusion-controlled process.[34]

3.4 Chronoamperometric studies

Chronoamperometry is an effective method for investigating the long-term stability and performance of the different electro catalysts (Pt/C, Pt/ZrO_2, Pt/ERGO and Pt/ZrO_2-ERGO and is used for samples immersed in 1M $HClO_4$ and 1M CH_3OH at 0.65 V for 3200 seconds. As can be seen in Fig. 4A, the current density for Pt/ZrO_2-ERGO remains higher than that of the other electro catalysts on the Pt/C, Pt/ZrO_2,Pt/ERGO, Pt/ZrO_2-ERGO modified electrodes throughout the whole test range. Results indicate that the former is more active than the latter in relation to methanol oxidation. There is a slight current decay due to the unavoidable formation of Pt adsorbed reaction intermediates during methanol oxidation and enhanced electrocatalytic activity. Table 1 shows electrochemical properties of Pt/C, Pt/ZrO_2, Pt/ERGO and Pt/ZrO_2-ERGO. The current density at 1500 s is 6.12 mA mg^{-1} for Pt/ZrO_2-ERGO, much higher than for the Pt/ERGO (3.88 mA mg^{-1}), Pt/ZrO_2 (1.2 mA mg^{-1}) and Pt/C (0.5 mA mg^{-1}). Pt/ZrO_2-ERGO has the best stability during methanol oxidation out of all the electro catalysts. It should be noted that the current decay is slower for Pt/ZrO2-ERGO than for Pt/ERGO, indicating that the incorporation of Pt into ZrO_2-ERGO reduce the poisonous effect and enhances the catalytic stability during methanol oxidation. The process can be summarized as follows. Firstly, ZrO_2 offers more active sites for improved deposition of Pt particles, which results in a larger active surface area on the Pt/ZrO_2-ERGO electro catalysts. Secondly, the hydroxyls adsorbed on the ZrO_2 surface may act to remove the adsorbed carbonyl from the surface of the Pt, allowing the dissociation-adsorption of methanol to proceed more quickly. In addition, the Pt particles on the surface of the ZrO_2-ERGO electro catalysts may act as active centers during the process of methanol oxidation. The surface reaction of CO with OH probably takes place in the following form (5):

$$Pt\text{-}CO_{ads} + ZrO_2\text{-}OH_{ads} \rightarrow Pt + ZrO_2 + CO_2 + H_2O + e^{-}. \quad (5)$$

By this means the CO-poisoned Pt/ZrO_2-ERGO electro catalysts can be regenerated, thereby partially eliminating the CO poisoning effect.

Fig. (4)

3.5 Electrochemical impedance spectroscopy (EIS) studies

Fig. 4B shows the EIS spectra and Nyquist plots (Z′ versus "-Z") for the (a) Pt/C, (b) Pt/ERGO, (c) Pt/ZrO_2 and (d) Pt/ZrO_2-ERGO/GCE electrodes in 1M $HClO_4$ + 1M CH_3OH aqueous solutions at a potential of 0.5 V for comparison with the saturated Ag/AgCl, and the corresponding Nyquist plots shown in Fig. 4B. Obviously, significant differences in the impedance spectra are observed for different electrodes. Fig. 4B illustrates the Nyquist diagrams for the large charge transfer resistance R_{et} of 948 Ω for the Pt/ERGO/GCE which can be attributed to the high C/O ratio making the molecules less electrically conductive and adding an additional increased electron transfer resistance for the GCE. A further decrease in the R_{et} value to 448 Ω was observed after the deposition of Pt/ZrO_2 nanoparticles on the GCE surface (Fig. 4B, curve c). The results confirm that the R_{et} value of the Pt/ERGO modified electrode is larger than that of the Pt/ZrO_2 modified electrode. After the assembly of the Pt particles on the ZrO_2 - ERGO layer, there was a dramatic decrease in the semicircular diameter 208.4 Ω (a), attributable to the Pt obstructing the electron transfer tunneling and higher electrocatalytic activity leading towards methanol electro oxidation. The Pt/ZrO_2-ERGO has a low C/O ratio. There was a remarkable decrease in the R_{et} value of the Pt/ZrO_2-ERGO after the Pt particles grew on the ZrO_2-ERGO/GCE. It can be seen that the semicircular diameter of the Pt/C modified electrode is much larger than that of the Pt/ZrO_2-ERGOelectrode. This suggests that the Pt/ZrO_2-ERGO

composite film has higher stability as an electro catalyst. In other words, this result indicates higher electrocatalytic activity towards methanol oxidation.

It is well known that the long-term cyclic stability of electro catalysts is necessary for practical applications. The long-term stability of Pt/ZrO_2-ERGO electro catalysts was investigated by using the cyclic voltammetric method after immersion in a 1M $HClO_4$ + 1M CH_3OH solution for 200 cycles. The results are presented in Fig 5A. It can be seen that the peak current decreased gradually with successive scans. By the 200th scan the peak current was about 92% that of the first scan. The loss of the peak current during methanol oxidation may be the result of the consumption of methanol over the long time it took for the cyclic voltammetry scans. The Pt/ZrO_2-ERGO electro catalysts exhibits excellent long-term cycle stability, which further suggests that that they are favorable candidates for use in DMFCs (See Fig S4). Which is substantially higher stability than that of the (a) Pt/C (36 %), (b) Pt/ZrO_2 (42 %), and (c) Pt/ERGO (66 %) (See table 1). After the long-term cyclic voltammetry scan experiments, the Pt/ZrO_2-ERGO electro catalysts were immersed in deionized water for about 1 week after which the methanol oxidation experiment was performed again. Excellent catalytic activity for methanol oxidation was obtained, indicative of the good long-term stability and storage properties of the prepared Pt/ZrO_2-ERGO electro catalysts.

Fig. (5)

Fig. 5B shows the polarization and performance curves of the direct methanol fuel cell assembled with the Pt/ZrO_2-ERGO electro catalyst as the anode and a commercial Pt/C as the cathode. The cell was operated at 30 ºC in the presence of 1M $HClO_4$ + 1M CH_3OH aqueous solutions. Here, Nafion 112 was used as the membrane. The modified Pt/ZrO_2-ERGO electrode

provided better power performance, by as much as 125 mW cm^{-2} compared to the commercial Pt/C (80 mW cm^{-2}). The improved performance can be attributed to the high oxygen reduction activity and the enhanced tolerance towards the oxidation of methanol transferred from the anode to the cathode through the Nafion membrane. In addition, the open-circuit voltage (VOC) for Pt/ZrO_2-ERGO was higher than that for the Pt/C. The VOC of the methanol fuel cell was approximately 0.68 V, with a maximum power density of 125mW cm^{-2} achieved. Further research is underway to improve the power density of the assembled direct methanol cell. The above results indicate that the Pt/ZrO_2-ERGO composite and Pt/C composite are excellent platforms for the development of direct methanol fuel cells.

4. Conclusion

In summary, we have demonstrated that Pt particles can be deposited on an ZrO_2-ERGO composite using a very simple electrodeposition method. ERGO is shown to be a good candidate for electro catalyst support because of its high surface area and high electrochemical performance. The Pt/ZrO_2-ERGO modified film exhibited better catalytic activity and stability for the electrooxidation of methanol than did the Pt/ERGO modified film, making it a promising choice for efficient electro catalysts in DMFCs. Furthermore, our approach can be extended to the preparation of other ZrO_2/Pt based particles on ERGO for electro catalysis or electrochemical sensors. These Pt/ZrO_2-ERGO materials demonstrated highly stable performance with greatly enhanced tolerance to electro catalyst poisoning, and better catalytic activity than other electro catalysts or Pt-based commercial electro catalysts. Finally, based on these results, we conclude that the Pt/ZrO_2-ERGO modified film provides a promising and less expensive alternative to using a methanol oxidation anode electro catalyst, which is helpful for easy electro oxidation.

Acknowledgements

The authors would like to express their appreciation for the financial support received from the Ministry of Science and Technology, Taiwan (Republic of China).

References

[1] R. Service, *Science* (New York, NY), 2002, **296**, 1222-1224.

[2] C.Y. Wang, *Chem. Rev.* 2004,**104**, 4727-4766.

[3] L. Gao, L. Ding, L. Fan, *Electrochim. Acta*, 2013, **106**, 159-164.

[4] B.Y. Xia, H.B. Wu, X. Wang, X.W. Lou, *J. Am. Chem. Soc.,* 2012, **134**, 13934-13937.

[5] H.C. He, P. Xiao, M. Zhou, F.L. Liu, S.J. Yu, L. Qiao, Y.H. Zhang, *Electrochim. Acta*, 2013, **88**, 782-789.

[6] J. Dong, E.K. Wang, *ACS Nano*, 2010, **4**, 547-555.

[7] J. Feng, Q. Zhang, A. Wang, J. Wei, J. Chen, J. Feng, *Electrochim. Acta*, 2014, **142**, 343-350.

[8] Z. Ji, X. Shen, G. Zhu, K. Chen, G. Fu, L. Tong, *J. Electroanal. Chem.,* 2012, **682**, 95-100.

[9] Y. Lei, B. Liu, J. Lu, R.J. Lobo-Lapidus, T. Wu, H. Feng, X. Xia, A.U. Mane, J.A. Libera, J.P. Greeley, *Chem. Mat.*2012, **24**, 3525-3533.

[10] A.K. Geim, K.S. Novoselov, *Nat Mater* 2007, **6**, 183-191.

401 [11] A.T. E. Vilian, S. Chen, Y. Chen, M. Ajmal Ali, F. M.A. Al-Hemaid, *Colloids Surf*. 2014,
402 **423**, 33-40.
403 [12] G. Shi, Z. Wang, J. Xia, S. Bi, Y. Li, F. Zhang, L. Xia, Y. Li, Y. Xia, L. Xia, *Electrochim.*
404 *Acta*, 2014, **142**, 167-172.
405 [13] L. Dong, R. Gari, Z. Li, M. M. Craig, S. Hou, *Carbon*, 2010, **48,** 781-787.
406 [14] T.Q. Xu, Q.L. Zhang, J.N. Zheng, Z.Y. Lv, J. Wei, A.J. Wang, J.J. Feng, *Electrochim. Acta*,
407 2014, **115**, 109-115.
408 [15] Y.M. Li, L.H. Tang, J.H. Li, *Electrochem. Commun.* 2009, **11**, 846-849.
409 [16] S. Yu, Q. Liu, W. Yang, K. Han, Z. Wang, H. Zhu, *Electrochim. Acta*, 2013, **94**, 245-251.
410 [17] K. Sato, H. Abe, S. Ohara, *J. Am. Chem. Soc.* 2010, **132**, 2538-2539.
411 [18] R. Sandoval, A.M. Cooper, K. Aymar, A. Jain, K. Hristovski*, J. Hazard. Mater*. 2011, **193**,
412 296-303.
413 [19] J.S. Wang, J.Y. Xi, Y.X. Bai, Y. Shen, J. Sun, L.Q. Chen, W.T. Zhu, X.P. Qiu, *J. Power*
414 *Sources,* 2007, **164**, 555-560.
415 [20] F. Lupo, R. Kamalakaran, C. Scheu, N. Grobert, M. Ruhle, *Carbon*, 2004, **42**, 1995-1999.
416 [21] D.J. Guo, X.P. Qiu, W.T. Zhu, L.Q. Chen, *Appl. Catal. B* 2009, **89**, 597-601.
417 [22] R. Liang, M. Deng, S. Cui, H. Chen, J. Qiu, *Mater. Res. Bull.* 2010, **45,** 1855-1860.

[23] Y. Shan, L. Gao, Nanotechnology, 2005, **16**, 625-630.

[24] D.C. Marcano, D. Kosynkin, J.M. Berlin, A. Sinitskii, Z. Sun, A. Slesarev, L.B. Alemany, W. Lu, J.M. Tour, *ACS nano*, 2010, **4**, 4806-4814.

[25] B. G. Choi, H.S. Park, M. H. Yang, Y.M. Jung, S. Y. Lee, W. H. Hong, T.J. Park, *Nanoscale,* 2010, **2**, 2692-2697.

[26] Y. Xu, H. Bai, G. Lu, C. Li and G. Shi, *J. Am. Chem. Soc.*, 2008, **130**, 5856-5857.

[27] Y. Li, K. Sheng, W. Yuan, G. Shi, *Chem. Commun.*, 2013, **49,** 291-293.

[28] Q. Wu, Y. X. Xu, Z. Y. Yao, A. R. Liu and G. Q. Shi, *ACS Nano*, 2010, **4,** 1963-1970.

[29] C.J. Cai, M.W. Xu, S.J. Bao, C. Lei, D.Z. Jia, *RSC Adv.,* 2012, **2,** 8172-8178.

[30] Z. Sun, Z. Rong, Y.Wang, Y. Xia, W. Du, Y. Wang, *RSC Adv.*, 2014, **4,** 1874-1878.

[31] A.A. Ensafi, M. Jafari-Asl, B. Rezaei, *Electrochim. Acta*, 2014, **130**, 397-405.

[32] G. Girishkumar, M. Rettker, R. Underhile, D. Binz, K. Vinodgopal, P. Mcginn, *Langmuir*, 2005, **21**, 8487-8494.

[33] L.A. Estudillo-Wong, A.M. Vargas-Gómez, E.M. Arce-Estrada, A. M. Robledo, *Electrochim. Acta*, 2013, **112**,164-170.

[34] W. Ye, Y. Chen, Y. Zhou, J. Fu, W. Wu, D. Gao,F. Zhou, C.Wang, D. Xue, *Electrochim. Acta*, 2014,142,18-24.

[35] L. Dong, R. Gari, Z. Li, M. M. Craig, S. Hou, *Carbon*, 2010, **48,** 781-787.

[36] Y. Li, W. Gao, L. Ci, C. Wang, P. M. Ajayan, *Carbon*, 2010, **48,** 1124-1130.

[37] C. Ma, W. Liu, M. Shi, X. Lang, Y. Chu, Z. Chen, D. Zhao, W. Lin, C. Hardacre, *Electrochim. Acta*, 2013, **114**,133-141.

[38] Z. Li, L. Zhang, X. Huang, L. Ye, S. Lin, *Electrochim. Acta*, 2014, **121**, 215-222.

[39] S. Yu, Q. Liu, W. Yang, K. Han, Z. Wang, H. Zhu, *Electrochim. Acta*, 2013, **94**, 245-251.

452

453

454 **Figure captions**

455 Scheme 1. Schematic representation of methanol oxidation taking place at Pt/ZrO_2-ERGO
456 electro catalyst modified electrode.

457 **Fig. 1** SEM images of the (A) ERGO/ITO, (B) Pt/ERGO/ITO, (C) Pt/ZrO_2-ERGO/ITO modified
458 films, and EDX spectra of the (D) ERGO/ITO, (E) Pt/ERGO /ITO, and (F) ZrO_2-ERGO/ITO and
459 HRTEM image of the (G) Pt/ZrO_2-ERGO modified film.

460 **Fig. 2** (A) FTIR spectra of the (a) GO and (b) Pt/ZrO_2-ERGO composite, (B) Raman spectra of
461 the (a) GO, (b) ZrO_2-ERGO and (c) Pt/ZrO_2-ERGO composite, and XRD analysis results of the
462 Pt/ZrO_2-ERGO/ITO modified film.

463 **Fig 3**. (A) CV curves of the (a) Pt/C, (b) Pt/ZrO_2, (c) Pt/ERGO and (d) Pt/ZrO_2-ERGO modified
464 electrodes in 1 M $HClO_4$ without methanol (scan rate = 50 mV s^{-1}). (B) Cyclic voltammograms
465 of the (a) Pt/C, (b) Pt/ZrO_2, (c) Pt/ERGO and (d)) Pt/ZrO_2-ERGO modified electrodes in 1 M
466 $HClO_4$ with 1 M CH_3OH (scan rate = 50 mV s^{-1}).

467 **Fig. 4** (A) Chronoamperograms of the (a) Pt/C, (b) Pt/ZrO_2, (c) Pt/ERGO, and (d) Pt/ZrO_2-
468 ERGO electrodes at 0.65 V in 1M $HClO_4$ + 1M CH_3OH aqueous solutions. (B) EIS of the (a)
469 Pt/C, (b) Pt/ERGO/GCE, (c) Pt/ZrO_2/GCE and (d) Pt/ZrO_2-ERGO/GCE electrodes in 1M $HClO_4$
470 + 1M CH_3OH aqueous solutions at 0.5 V. Frequency range: 0.1 Hz to 100 kHz. Inset: Randles
471 equivalence circuit.

472

Fig. 5 (A) Cyclic voltammograms of Pt/ZrO_2-ERGO with 1 cycle (a), 50 cycles (b), 100 cycles (c), and 200 cycles (d) in a nitrogen saturated solution of 1M $HClO_4$ containing 1 M CH_3OH at a scan rate of 50 mV s^{-1}. (B) Cell polarization and power density curves obtained using Pt/ZrO_2-ERGO catalyzed anode and an Pt/C black catalyzed cathode in electrolyte 1M $HClO_4$ + 1M CH_3OH aqueous solutions; Nafion 112; cell temperature 30°C.

491

492

493

494 **Figures**

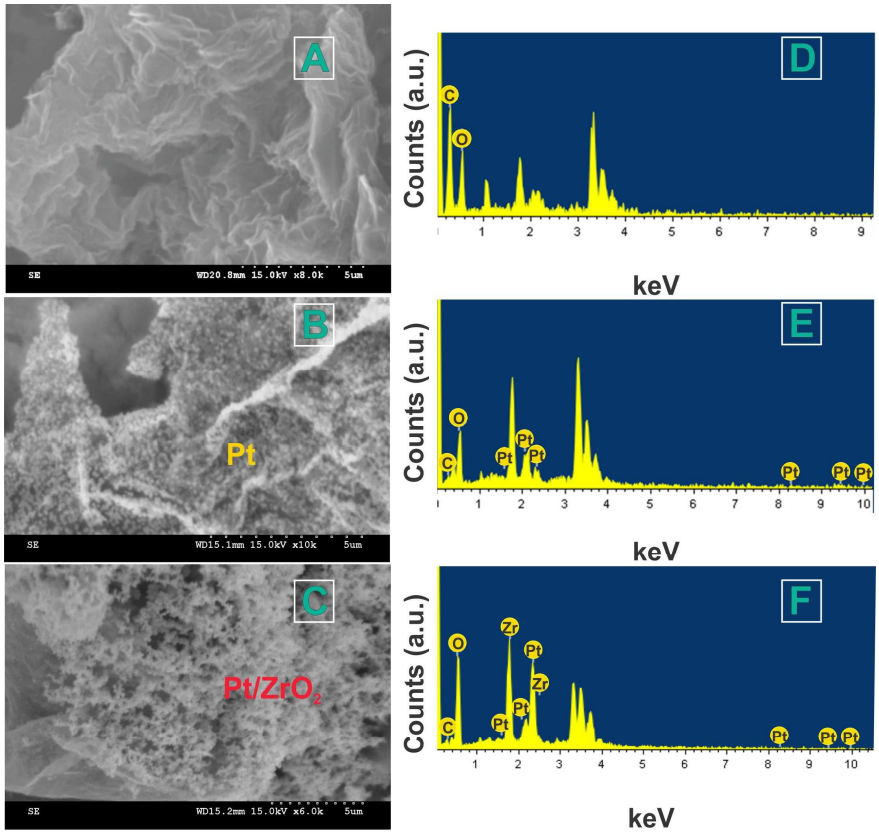

495

496

497 Fig **1)**

498

499

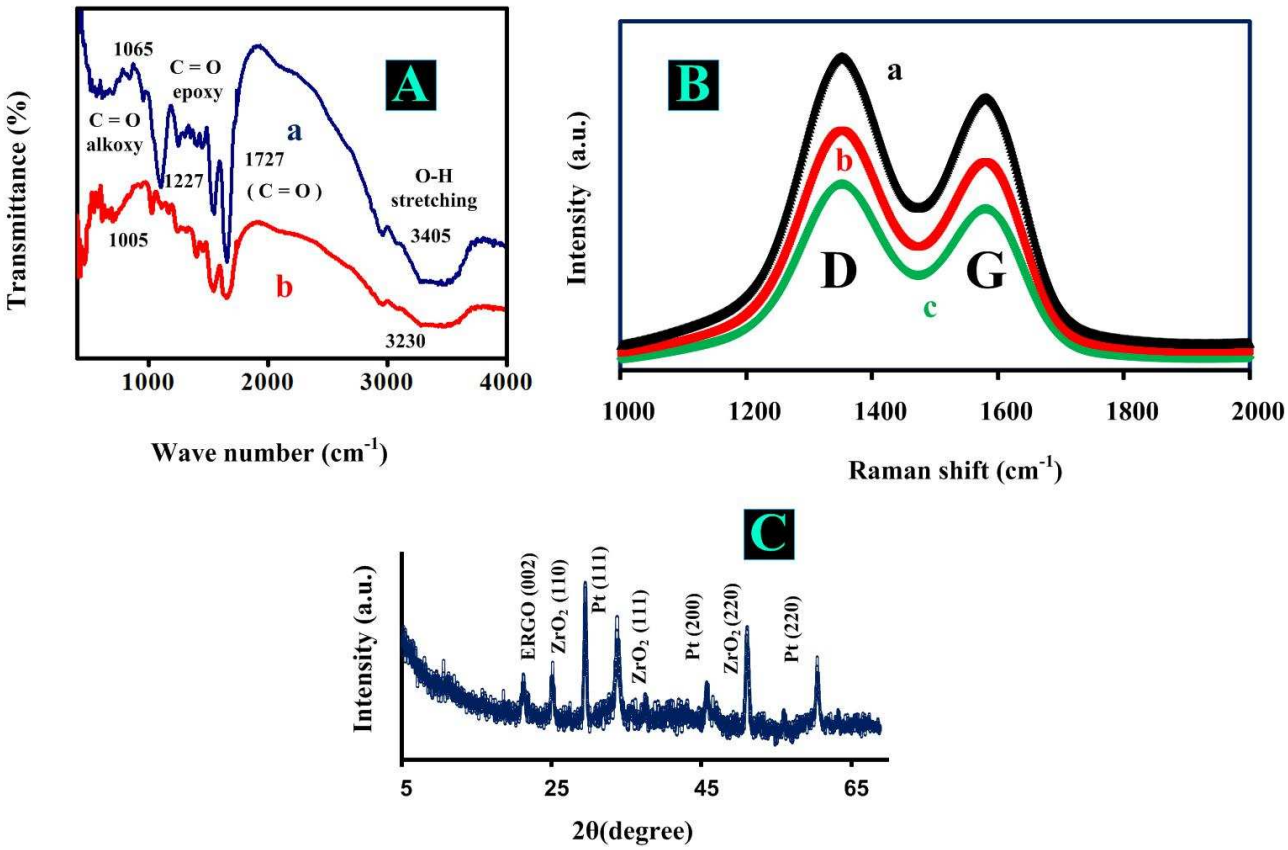

500

501

502 **Fig 2)**

503

504

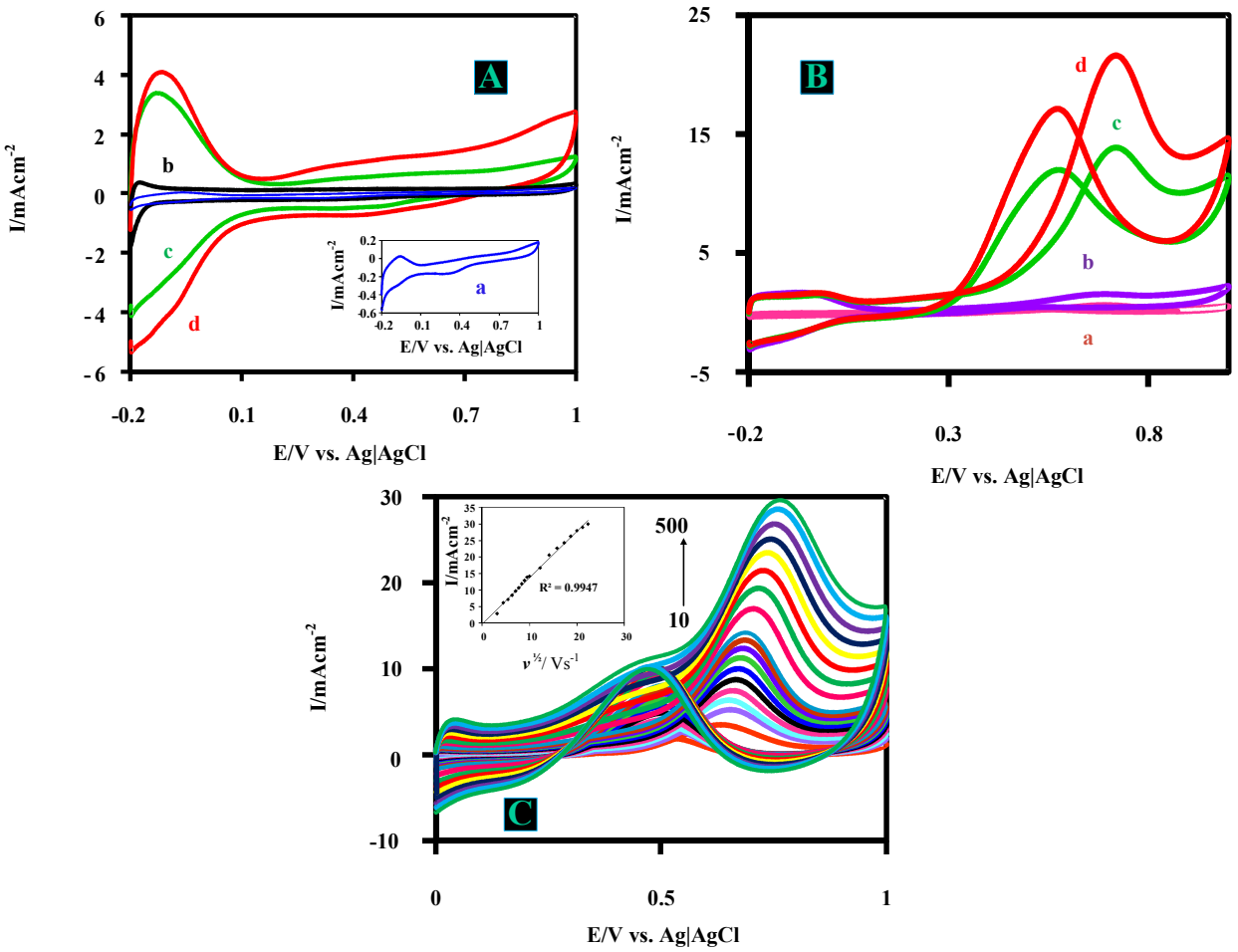

505

506 **Fig 3)**

507

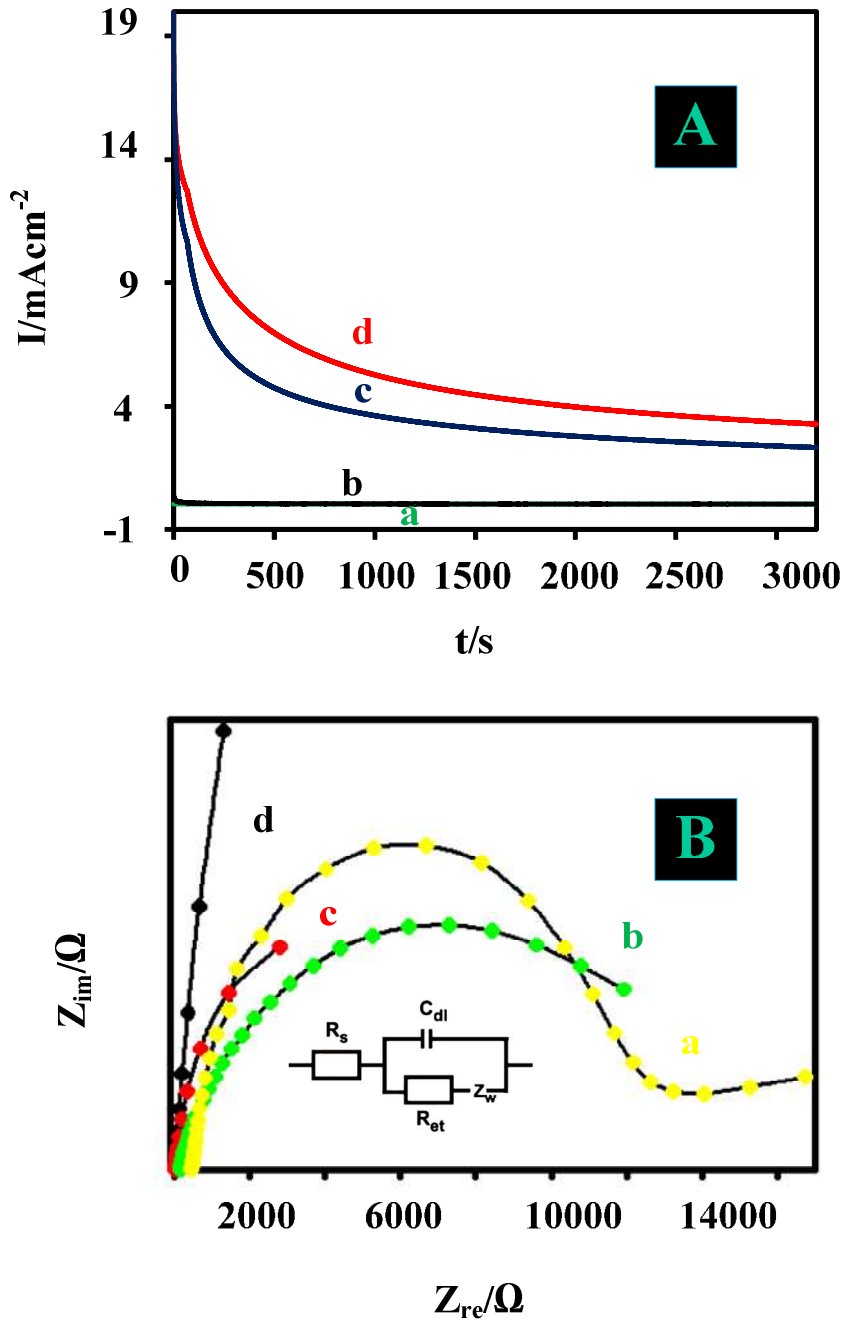

508

509

510 **Fig 4)**

511

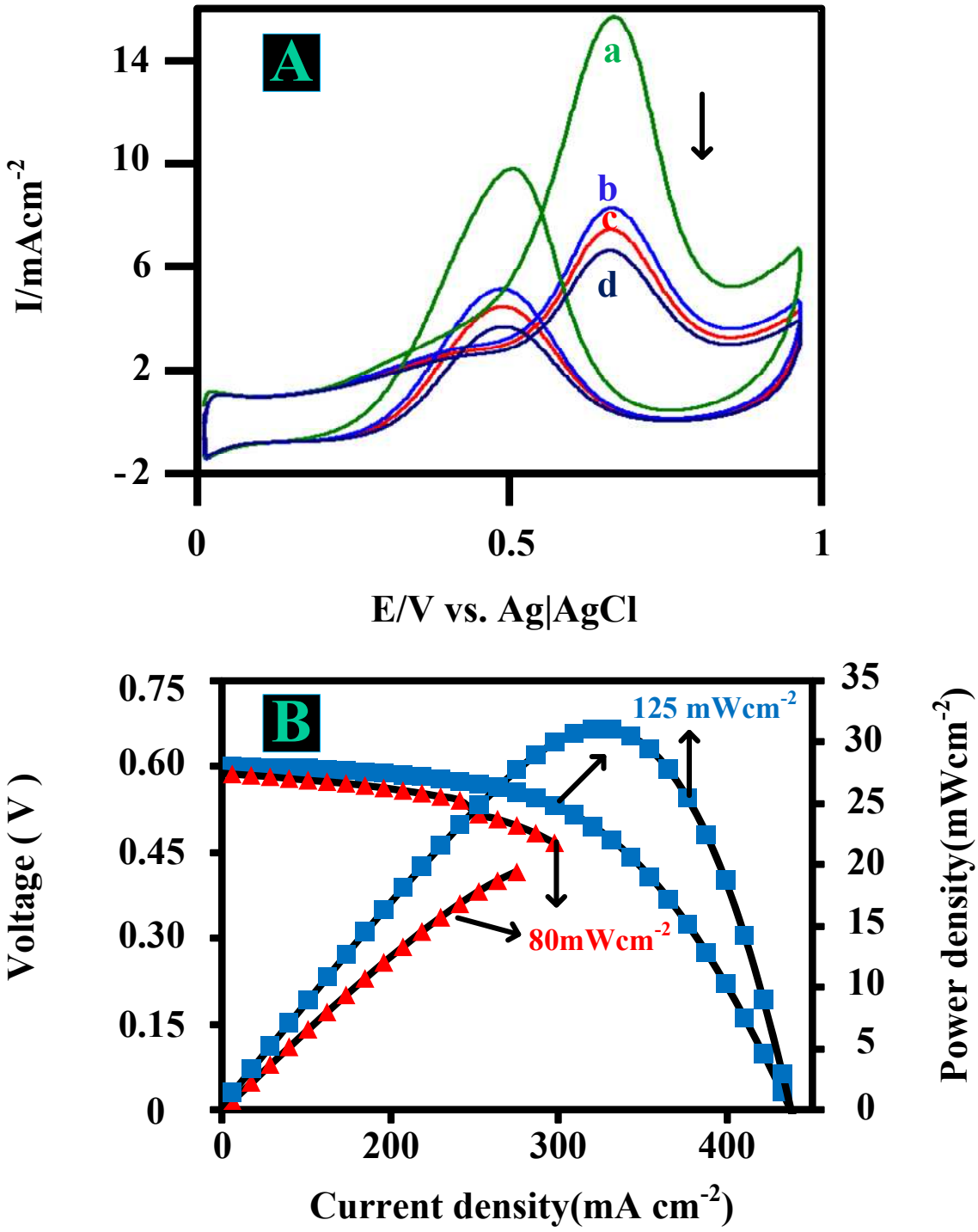

512

513 **Fig 5)**

514

Table 1.

Electrochemical properties of different electro catalyst.

Electro catalyst	Onset Potential (V)	EAS (m^2/g)	I_f/I_b	I a (mA)	Normalized current b (%)
Pt/ZrO_2-ERGO	0.335	68.2	1.92	6.12	92
Pt/ERGO	0.406	42.93	1.12	3.88	66
Pt/ZrO_2	0.491	36.13	1.02	1.2	42
Pt/C	0.535	34.02	0.98	0.5	36

[a]I is the the residual current at 0.65 V after 1500 s.

[b]Normalized current (%) is the percentage of the peak current of the 200th cycle compared to the maximum peak current.

528 Table 2. Comparison of the performance of the proposed Pt /ZrO_2-ERGO electro catalysts with

529 other electro catalysts.

Samples	Onset Potential (V)	EAS (m^2/g)	I_f/I_b	Ref
Pt /ZrO_2-ERGO	0.480	68.2	1.92	This work
Pt-Ru-graphite	0.500	-	1.52	[35]
Pt/MWCNT	0.300	33.43	0.72	[36]
Pt-reduced graphene oxide-supported WC nanocrystallites	0.250	253.12	1.26	[37]
Pt/graphene nanosheets -β-cyclodextrin	0.350	36.20	1.32	[38]
Pt 7% CeO_2/Graphene	0.659	66.4	1.48	[39]

530 I_f/I_b represents the ratio between the forward and backward anodic peak currents.

531

532

533

534

535

536

537

538